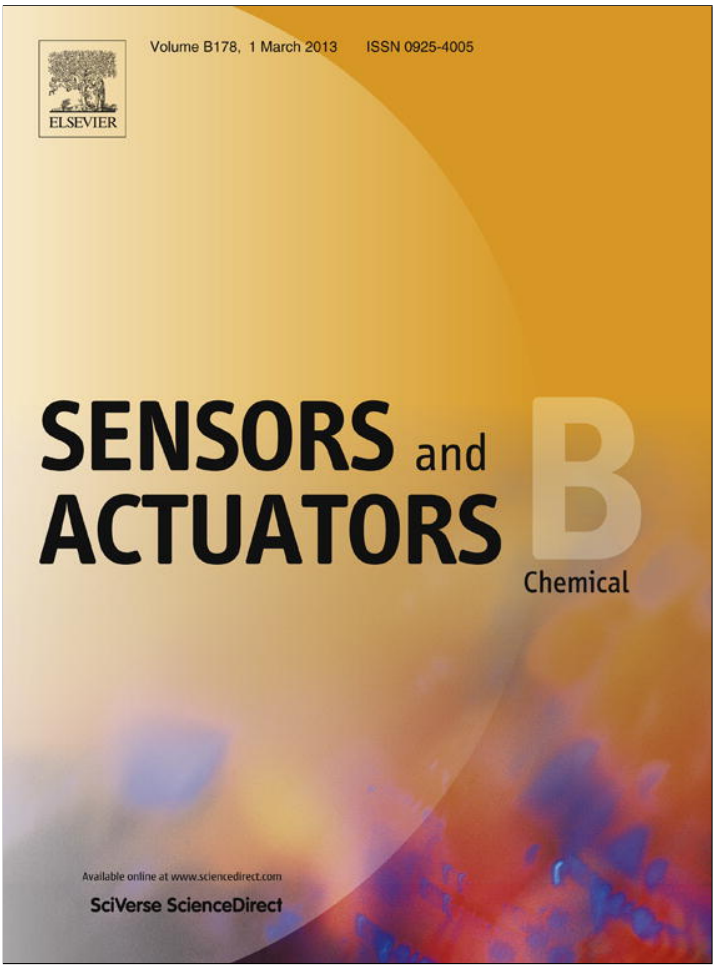

Sensors and Actuators B 178 (2013) 155–162

Contents lists available at SciVerse ScienceDirect

Sensors and Actuators B: Chemical

journal homepage: www.elsevier.com/locate/snb

A ratiometric fluorescence chemosenser for Hg^{2+} based on Primuline and layered double hydroxide ultrafilms

Hao Chen, Xiaolan Ji, Shitong Zhang, Wenying Shi*, Min Wei, David G. Evans, Xue Duan

State Key Laboratory of Chemical Resource Engineering, Beijing University of Chemical Technology, Beijing 100029, PR China

ARTICLE INFO

Article history:
Received 17 October 2012
Received in revised form
10 December 2012
Accepted 18 December 2012
Available online 29 December 2012

Keywords:
Layered double hydroxide
Primuline
Ultrathin film
Ratiometric fluorescence
Chemsensor

ABSTRACT

The fabrication of fluorescence indicator/layered double hydroxide (LDH) ultrathin films (UTFs) by alternate assembly of Primuline and Mg-Al LDH nanosheets using the layer-by-layer (LBL) deposition technique has been reported, and their application as a raitometric fluorescence chemosensor for Hg^{2+} is demonstrated. The Primuline/LDH UTFs show a stepwise and regular growth of upon increasing deposition cycles proved by UV–vis absorption and fluorescence emission spectroscopy, and a periodical layered structure perpendicular to the substrates with a thickness of 2.41–2.48 nm per bilayer observed by X-ray diffraction and scanning electron microscopy. Furthermore, a linear correlation between the fluorescence intensity ratio (I_{422}/I_{377}) of the UTF and the concentration of Hg^{2+} is obtained ($I_{422}/I_{377} = 2.63–0.01c$ nM, $r^2 = 0.99$), with a detection limit of 0.13 pM. The results have also exhibited that the ratiometric fluorescence chemosensor possess a good repeatability, high stability (light, storage and mechanics) as well as excellent selectivity. In addition, the mechanism of measurement–regeneration cycle for the ratiometric fluorescence chemosensor indicates Hg^{2+} enters/departs from the Primuline/LDH UTF giving rise to reversible change in chemical composition, surface morphology and fluorescence anisotropy of the UTF. Therefore, this work provides new opportunities for fabrication and application of chromophore/LDH UTFs as ratiometric fluorescence chemosensors.

1. Introduction

Mercury contamination in natural waters, soil and food due to mercury widespread throughout environment (coal-fired power plants, waste incinerators, chloro-alkali plants, gold mining, and oceanic and volcanic emission) is a global problem [1], which cause permanent damage diseases including cognitive and motion disorders [2]. Thus, it is quite imperative to detect mercury ions with sensitive, rapid and selective [3]. In general, traditional analytical techniques like atomic absorption/emission spectroscopy or inductively coupled plasma mass spectrometry are costly and time-consuming methods, which require complicated, multistep sample preparation and/or sophisticated instrumentation and are not convenient for "in the field" applications [4]. Fluorescence spectroscopy is a powerful method to detect ions and neutral molecules because of its high sensitivity, selectivity, fast-response and low cost [5]. However, most of these fluorescence determinations were designed to exhibit enhancement of the fluorescence intensity at only one wavelength, which may cause difficulty in quantitative determination and bio-imaging due to the background interference [6]. Ratiometric fluorescence probes are better choices that can overcome this particular limitation, because they allow quantitative detection of the analyte by measuring the ratio of emission at two different wavelengths. Recently, considerable attention has been focused on development of ratiometric fluorescence sensors for sensing and recognition of environmentally and biologically important heavy and transition metal ions for achieving higher sensitivity, rapid and reversible detection [7].

Organic fluorescence small molecular and polymer were usually used as a fluorescence sensors probe in detection systems of heavy and transition metal ions. Nevertheless, among these probes, chemical reactions between organic molecular and metal ions partly weakened the selectivity of this determination. In addition, organic fluorescence molecules were vulnerable to photobleaching, which made specific detection more difficult. Thus, the fluorophore indicators are generally immobilized in matrix for the purpose of obtaining fluorescence sensors with stable lifetime and signal. Most fluorescence indicators were immobilized in a suitable, proton-permeable sol-gel polymer matrix [8]. However some inherent demerits for the polymer, such as relatively poor thermal or optical stability as well as toxicity, limit the practical application of fluorescence sensors to date. Therefore, it is essential to search for novel materials to immobilize the fluorophore indicator for achieving fluorescence sensors with high stability and environmental compatibility.

* Corresponding author. Tel.: +86 10 64412131; fax: +86 10 64425385.
E-mail address: shiwy@mail.buct.edu.cn (W. Shi).

0925-4005/$ – see front matter © 2012 Elsevier B.V. All rights reserved.
http://dx.doi.org/10.1016/j.snb.2012.12.075

Among the inorganic matrices for organic fluorescence molecules, the 2-dimensional layered double hydroxide (LDH) materials have attracted much attention. The LDHs generally expressed as $[M^{II}_{1-x}M^{III}_{x}(OH)_2](A^{n-})_{x/n}\cdot mH_2O$ (where M^{II} and M^{III} are divalent and trivalent metals respectively, and A^{n-} a n-valent anion), represent a large versatility in terms of their ability for constructing 2D-organized intercalated compounds [9]. They are available as both naturally occurring minerals and synthetic inorganic materials, which have been widely used in the fields of catalysis, separation process, biology and medicine [10]. The delamination of LDH into nanosheets as building blocks and preparation of inorganic/organic fluorophore ultrathin films (UTFs) has been reported. This inspires us to challenge the goal of fabricating fluorescence chemosensors *via* alternate assembly of positively charged LDH nanosheets and negatively charged fluorophore indicator with the layer-by-layer (LBL) technique, which exhibit the following advantages: (1) the positively charged LDH nanosheet provides fluorescence anions with an ordered microenvironment to isolate the anions between adjacent layers, suppressing chromophore aggregation and reducing fluorescence quenching [11]; (2) the LDH nanosheets provide a confined and stable microenvironment for the immobilization of fluorophore indicator, which meet the requirement of long-term application; (3) the rigid and confined space imposed by LDH monolayers can suppress the thermal vibration and rotation of fluorescence anions relating to the nonradiative relaxation process of their exciting states.

Primuline and their derivatives are yellow fluorescence dyes, which were used early in the fluorescence tracer due to their tunable spectral properties, large molar extinction coefficients, and high quantum yields [12]. Nevertheless, the aggregation of Primuline dyes in the solid state usually leads to fluorescence quenching, which greatly restricts their application in solid-state devices. Therefore, how to improve their luminescence performances remains a challenge. In this work, an ordered alternate assembly of Primuline and exfoliated Mg-Al-LDH nanosheet has been achieved to fabricate the $(Primuline/LDH)_n$ (n = 5–30) ultrathin films (UTFs) by the LBL method. The obtained UTFs show well defined absorption and fluorescence properties with long-range ordered structure and higher thermal/chemical stability than the pristine Primuline samples. In addition, they were successfully demonstrated as ratiometric fluorescence chemosensor for Hg^{2+}, which exhibits a broad linear response range for Hg^{2+} solution (2.5–100 nM), low detection line (0.13 pM), good repeatability (RSD less than 3% in 20 consecutive measurements), high stability (light, storage and mechanics) as well as excellent selectivity. Therefore, the novel strategy in this work provides a facile approach for the fabrication of luminescence film, which can be potentially applied in the field of ratiometric optical sensors.

2. Experimental

2.1. Materials

The Primuline (biochemistry grade) was purchased from Sigma–Aldrich Company. Analytical grade chemicals including $Mg(NO_3)_2$, $Al(NO_3)_3$, NaOH, $Ca(NO_3)_2$, $Cd(NO_3)_2$, $Hg(NO_3)_2$, $Co(NO_3)_2$, $Cu(NO_3)_2$, $Zn(NO_3)_2$, $Pb(NO_3)_2$, $Mn(NO_3)_2$, $Ni(NO_3)_2$, HNO_3, H_2SO_4, H_2O_2, C_2H_5OH, formamide and ethylenediamine tetraacetic acid (EDTA) were used without further purification. The deionized and decarbonated water was used in all the experimental processes.

2.2. Fabrication of the $(Primuline/LDH)_n$ UTFs

The Mg_2-Al-NO_3 LDH precursor was synthesized by the hydrothermal method reported previously [13]. A 0.1 g of Mg-Al-LDH was shaken in 100 mL of formamide solution for 24 h to obtain a colloidal suspension of exfoliated Mg-Al-LDH nanosheets. The quartz glass substrate was cleaned in concentrated NH_3/30% H_2O_2 (7:3) and concentrated H_2SO_4 for 30 min each. After each procedure, the quartz substrate was rinsed and washed thoroughly with deionic water. The substrate was dipped in a colloidal suspension (0.1 g mL^{-1}) of LDH nanosheets for 10 min followed by washing thoroughly, and then the substrate was treated with a 100 mL of Primuline aqueous solution (0.025 wt%) for another 10 min followed by washing. Multilayer films of $(Primuline/LDH)_n$ were fabricated by alternate deposition of LDH nanosheets suspension and Primuline solution for n cycles. The resulting films were dried with a nitrogen gas flow for 2 min at 25 °C.

2.3. The response of Hg^{2+} measurement

The Hg^{2+} solutions with different concentrations were prepared by dissolving $Hg(NO_3)_2$ in a water/ethanol mixture solvent (1:1, v/v, 295 K). The ratiometric fluorescence chemosensor was immersed into a quartz cell with $Hg(NO_3)_2$ solution, and its response was recorded by a RF-5301PC fluorophotometer with a liquid holder.

2.4. Characterization techniques

The UV–vis absorption spectra were collected in the range from 220 to 800 nm on a Shimadzu T-9201 spectrophotometer, with the slit width of 1.0 nm. The fluorescence spectra were performed on a RF-5301PC fluorospectrophotometer with the excitation wavelength of 334 nm. The fluorescence emission spectra range in 350–650 nm, and both the excitation and emission slits were set to 3 nm. The photobleaching behavior was tested by the UV lighting with CHF-XQ 500W. Steady-state polarized photoluminescence measurements of the Primuline/LDH UTFs were recorded with an Edinburgh Instruments' FLS 920 fluorospectrophotometer. X-ray diffraction patterns (XRD) of the Primuline/LDH UTFs were recorded using a Rigaku 2500 VB2+PC diffractometer under the conditions: 40 kV, 50 mA, Cu Kα radiation (λ = 0.15 nm) step-scanned with a scanning rate of 2°/min, and a 2θ angle ranging from 2° to 65°. The morphology of thin films was investigated by using a scanning electron microscope (SEM ZEISS) with 20 kV accelerating voltage. The surface roughness was obtained by using the atomic force microscopy (AFM) software (Digital Instruments, version 6.12). X-ray photoelectron spectroscopy (XPS) measurement was performed with monochromatized A1 Kα exciting X-radiation (PHI Quantera SXM). The Raman spectra were obtained with 514.50 nm of excitation by using a confocal Raman microspectrometer (Renishaw Instruments Co. Ltd., RM2000) in the range 1000–2500 cm^{-1}.

3. Results and discussion

3.1. Characterization of the Primuline/LDH UTFs

3.1.1. Assembly of the UTFs

Fig. 1A shows the UV–vis absorption spectra of the $(Primuline/LDH)_n$ UTFs with various bilayer numbers (n) deposited on quartz substrates. A stepwise and regular film growth procedure is observed by the linear correlation between the absorption band of Primuline at ~233 and 355 nm (π–π^* transition) with n (inset in Fig. 1A). Compared with Primuline solution sample (Fig. S1), the absorption spectrum for the $(Primuline/LDH)_n$ UTFs is similar to Primuline solution, which excludes the aggregation of Primuline during the assembly process. The fluorescence quantum yield was calculated by the ratio between the fluorescence intensity (determined from the integral of the emission peak) and the absorbance at the excitation wavelength, I_{flu}/A_{exc} (Fig. S2) [14], from which the $(Primuline/LDH)_{25}$ UTF shows a higher value

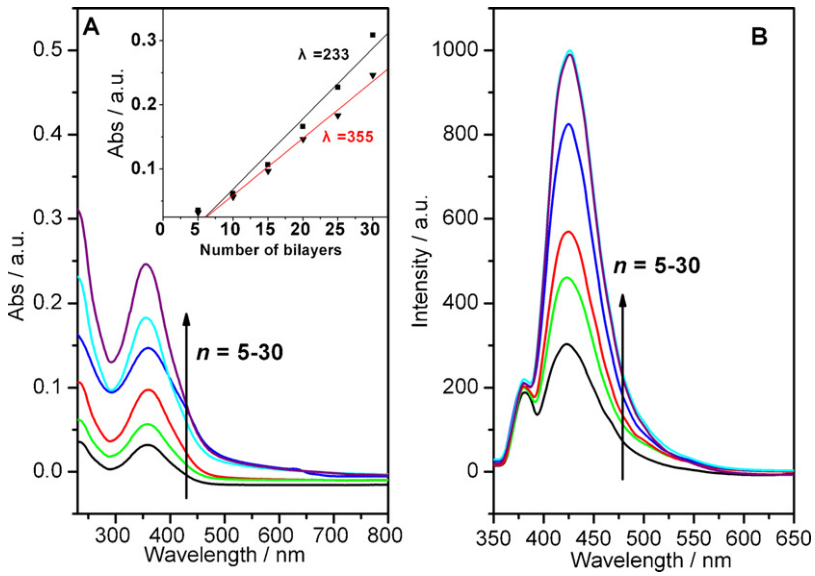

Fig. 1. (A) UV–vis absorption spectra of the $(Primuline/LDH)_n$ UTFs (n = 5–30) (inset: the linear relationship between absorbance at 233 and 355 nm and bilayer number n); (B) the fluorescence emission spectra of the $(Primuline/LDH)_n$ UTFs (n = 5–30).

than that of the solution (10^{-5} mol/L) and pure solid Primuline sample. This suggests that the rigid and confined space imposed by LDH monolayers can suppress the thermal vibration/rotation of Primuline relating to the nonradiative relaxation process of its exciting states. Fig. 1B displays that the fluorescence emission intensity of $(Primuline/LDH)_n$ UTFs at 422 nm consistent increase along with n from 5 to 25, while it shows no change with further increasing n to 30. In addition, the fluorescence emission intensity at 377 nm absents obvious change. The biggest fluorescence intensity ratio (I_{422}/I_{377}) located at the n = 25 (Fig. S3). The further monitor for the deposition process of the $(Primuline/LDH)_n$ UTFs was carried out by scanning electron microscopy (SEM). The approximately linear increase of the UTF thickness in the range 25–62 nm upon increasing the layer number (n = 10–25) confirms that the UTFs present uniform and periodic layered structure (Fig. S4).

3.1.2. Structural and morphological characterization

Fig. 2A shows a typical top view of SEM image for the $(Primuline/LDH)_{25}$ UTF, which displays the film surface is microscopically continuous and smooth. The SEM side view (Fig. 2B) of $(Primuline/LDH)_{25}$ UTF indicates the thickness is 62 nm, from which it can be estimated that the thickness of one bilayer $(Primuline/LDH)_1$ is ~2.48 nm. The AFM topographical image is shown in Fig. 2C, and the result indicates the value of root-mean-square (RMS) roughness is 3.46 nm, indicating a relatively smooth surface. The XRD patterns exhibit the characteristic reflection of the LDH structure with a (0 0 3) peak appearing as narrow, symmetric, strong lines at $2\theta = 3.98^\circ$, indicating the average repeating distance is ~2.41 nm, approximately consistent with the thickness augment per deposited cycle observed by SEM (2.48 nm). Moreover, this is also in agreement with the ideal single-layered arrangement model of the Primuline/LDH structure (Fig. S5).

3.2. The $(Primuline/LDH)_n$ UTFs as a ratiometric fluorescence chemosensor for Hg^{2+}

3.2.1. The response of $(Primuline/LDH)_n$ UTFs for Hg^{2+}

The significant fluorescence decrease (at 422 nm) and increase (at 377 nm) of the $(Primuline/LDH)_n$ UTFs are observed with presence of Hg^{2+} (Fig. 3A), displaying their feasibility as a ratiometric chemsensor. The response time of the $(Primuline/LDH)_n$ UTFs toward Hg^{2+} increases with the increase of film thickness, resulting from the reduced diffusion rate of Hg^{2+} in the film with larger thickness (Fig. S6). Taking into account both the fluorescence intensity ratio (Fig. S2) and response time, the $(Primuline/LDH)_{25}$ UTF sample was chosen in the following study. Moreover, from the fluorescence sensitivity of view, pH 7 was chosen as the best measurement condition (Fig. S7).

Fig. 3B shows the fluorescence intensity ratio is proportional to the Hg^{2+} concentration in the range 2.5–100 nM, with the following linear regression equation: $I_{422}/I_{377} = 2.63–0.01c$ (nM) with $r^2 = 0.99$. The absolute detection limit is 0.13 pM, which meets the requirement for Hg^{2+} detection in bottled water within U.S. EPA and World Health Organization (WHO) limit (~30 nM) [15]. The ratiometric fluorescence change of the UTF with the presence of Hg^{2+} is probably related to the binding between Primuline and Hg^{2+}, which will be further discussed in the next section.

3.2.2. Reversibility

The reversibility is a key factor for chemsensors from the viewpoint of practical application. To realize the reversibility of the chemosensor, the treated by Hg^{2+} UTF was immersed into a solution of EDTA (a metal ion chelator, 5 μM), and the fluorescence intensity at 422 and 377 nm of the UTF increased and decreased gradually respectively and recovered completely after 35 s (Fig. 4A), demonstrating the binding between Primuline and Hg^{2+} is chemically reversible. A good repeatability of the chemosensor was observed with RSD = 1.23% (EDTA) and RSD = 2.56% (Hg^{2+}) in 20 cycles by alternate immersion into two solutions with Hg^{2+} and EDTA respectively (Fig. 4B).

3.2.3. Stability

The stability of chemosensor is of major importance, since it leads to indicator leaching and/or signal drifting even the breakdown of sensor ability [16]. The fluorescence intensity ratio (I_{422}/I_{377}) of the $(Primuline/LDH)_{25}$ UTF as a function of bleaching time upon illumination by UV light is recorded (Fig. S8), with the Primuline solution as a comparison sample. It was found that the half-live of the $(Primuline/LDH)_{25}$ UTF sample (10 h) is far longer than that of the Primuline solution (50 min). The result indicates that the photostability of Primuline molecule is significantly

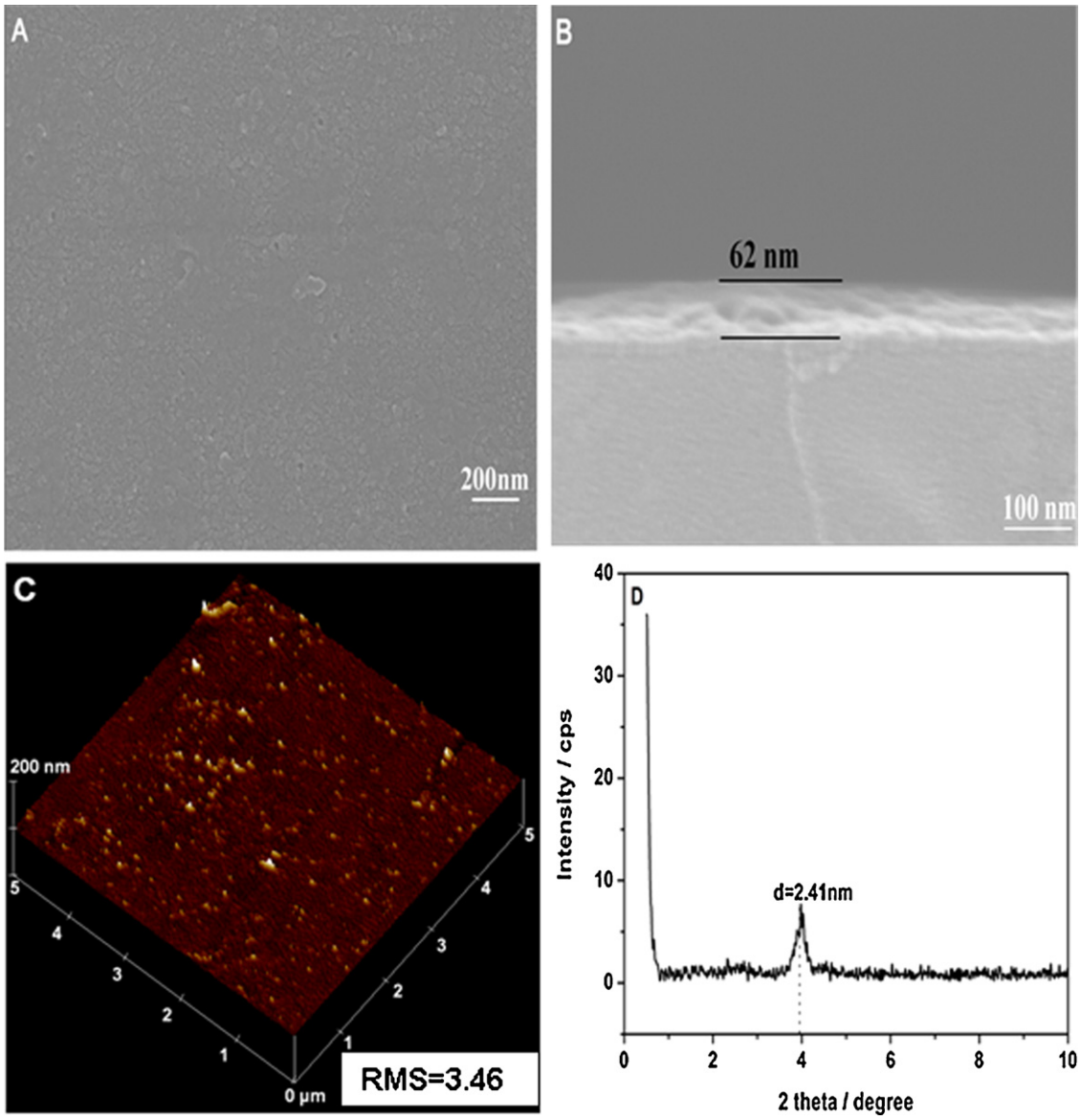

Fig. 2. (A) Top-view of SEM image, (B) side-view of SEM image, (C) tapping-mode AFM image and (D) XRD pattern of the $(Primuline/LDH)_{25}$ UTF.

enhanced in the LDH matrix. In addition, the ~96% of its initial fluorescence intensity remained after one month measurement, indicating the high storage stability of the chemsensor (Fig. S9). Moreover, the adhesion test of the UTF film to the substrate shows no delamination or peeling occurred on cross-cutting the surface (shown in Fig. S10).

3.2.4. Selectivity

For other competitive species, a high selectivity of the chemosensor toward analyte is obviously important. Fig. 5 shows the fluorescence intensity ratio (I_{422}/I_{377}) of the $(Primuline/LDH)_{25}$ UTF in solutions containing Ca^{2+}, Cd^{2+}, Pb^{2+}, Mn^{2+}, Fe^{2+}, Co^{2+}, Zn^{2+}, Cu^{2+}, Ni^{2+}, Cr^{3+}, Al^{3+} and Mg^{2+}, respectively. The results display the response of the UTF to other cations was very low compared with Hg^{2+}, and less change in the fluorescence intensity ratio of UTF for these interferential species (~5%) than Hg^{2+} (~65%) was observed. Furthermore, with the presence of a mixture of the above-mentioned metal ions (1 μM each), there is no significant influence on the fluorescence intensity ratio response to Hg^{2+}.

3.2.5. Determination of Hg^{2+} in real water samples

Application experiments are crucial for evaluating analytical performance of the chemosensor because of possible influence from naturally existing molecules and interferences. Two real samples (tap water and lake water collected from the Weiming lake in the Peking University) were used for the Hg^{2+} determination. Both the samples filtered through a 0.5 μL membrane showed no Hg^{2+} based on results of the elemental analysis. Thus, different concentrations of Hg^{2+} were respectively added in the water samples and then record the fluorescence intensity ratio (I_{422}/I_{377}) of the $(Primuline/LDH)_{25}$ UTF (Table 1). The satisfactory results for both the samples have been obtained, indicating that the $(Primuline/LDH)_{25}$ UTF can be potentially used as a ratiometric chemosensor for the detection of Hg^{2+} in the environmental field.

3.3. Studies on the mechanism of measurement–regeneration cycle

The process of fluorescence quenching and regeneration for the fluorescence chemosensor is shown in Scheme 1. The coordination of Hg^{2+} with Primuline in the UTF results from high

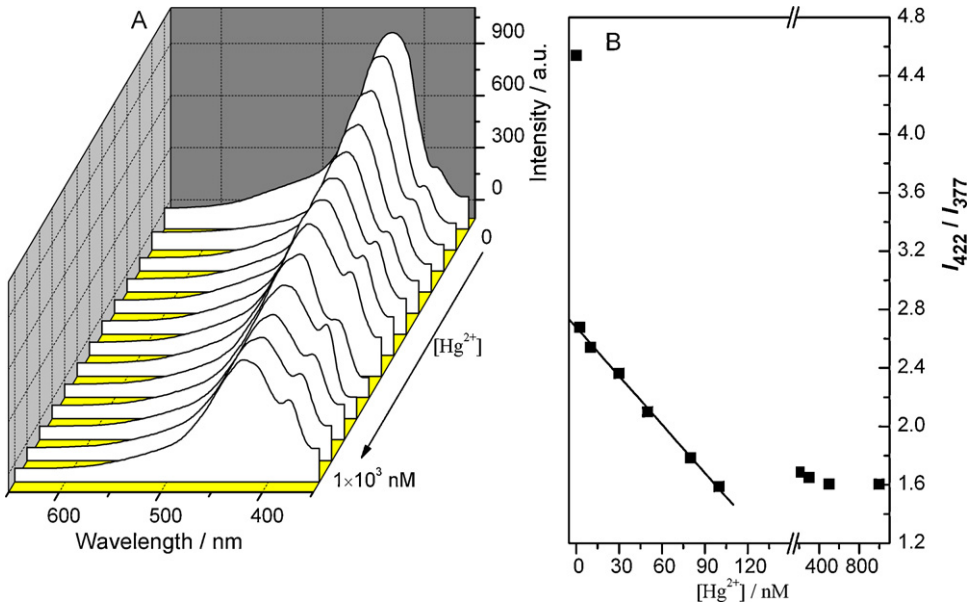

Fig. 3. (A) Emission spectra of the (Primuline/LDH)$_{25}$ UTF upon increasing Hg^{2+} concentration (293 K; λ_{ex} = 334 nm); (B) Hg^{2+} titration curve of the chemosensor for emission ratio at 422 and 377 nm (I_{422}/I_{377}).

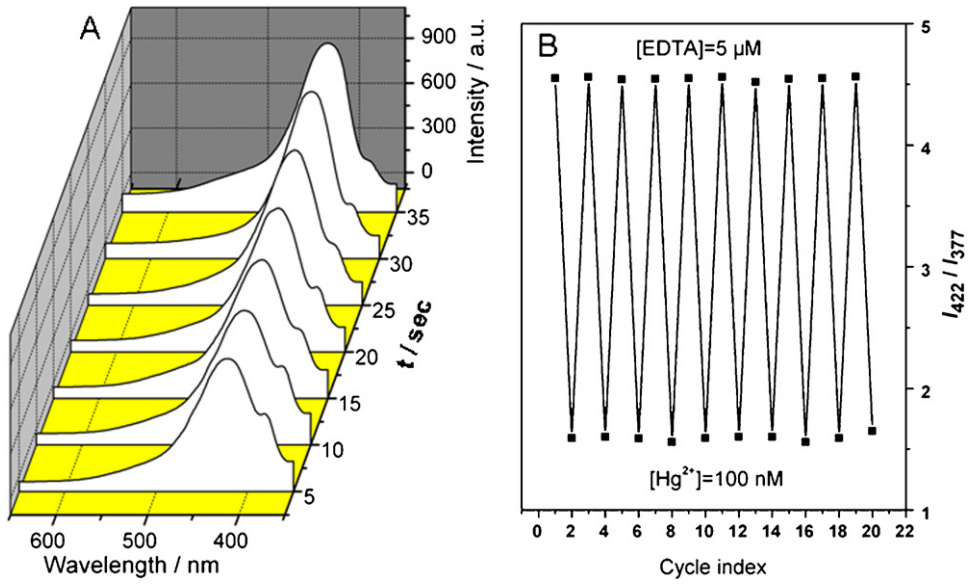

Fig. 4. (A) Emission spectra of the treated by Hg^{2+} chemosensor in EDTA (5 μM) as a function of time; (B) the reversibility of the chemosensor recorded by alternate measurement in two solutions of Hg^{2+} and EDTA respectively.

thermodynamic affinity of Hg^{2+} for typical S and N-chelate ligands and fast metal-to-ligand binding kinetics; while the decomplexation was rooted in the coordination of Hg^{2+} and EDTA owing to the much larger complex constant between EDTA and Hg^{2+} ($\log K \approx 21.8$) [17] than Primuline and Hg^{2+} ($\log K \approx 7$ based on the fit result of Stern–Volmer formula, see Fig. S11). This XPS and Raman measurement verified the process above (Fig. 6). The XPS spectrum after measurement of Hg^{2+} (Fig. 6A-b) displays signals

Table 1
Determination of Hg^{2+} in the tap and lake water.

Sample	Number	Hg^{2+} added (mol L^{-1})	Hg^{2+} found (mol L^{-1}) (mean[a] ± S.D.[b])	Recovery (%)
Lake water	No. 1	5.0×10^{-9}	$(5.04 \pm 0.12) \times 10^{-9}$	100.8
	No. 2	2.0×10^{-8}	$(2.03 \pm 0.21) \times 10^{-8}$	101.5
	No. 3	8.0×10^{-8}	$(8.12 \pm 0.11) \times 10^{-8}$	101.5
Tap water	No. 1	5.0×10^{-9}	$(5.01 \pm 0.09) \times 10^{-9}$	100.2
	No. 2	2.0×10^{-8}	$(1.98 \pm 0.15) \times 10^{-8}$	99.0
	No. 3	8.0×10^{-8}	$(8.10 \pm 0.13) \times 10^{-8}$	101.25

[a] Mean of three determinations.
[b] Standard deviation.

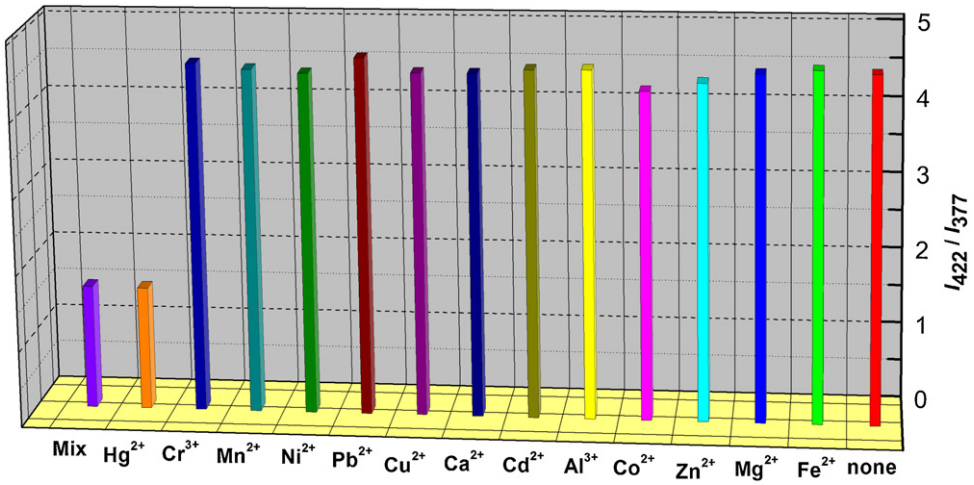

Fig. 5. The fluorescence intensity ratio (I_{422}/I_{377}) of the (Primuline/LDH)$_{25}$ UTF induced by indicated metal cations (1 μM respectively); mix = a mixed solution containing all the tested cations (1 μM each), none = pure water solution. Indicated values are means of three measurements with the standard error less than 3%.

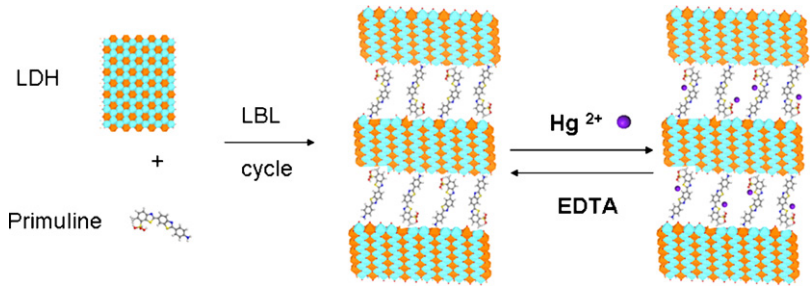

Scheme 1. The schematic representation for the measurement–regeneration cycle of the UTF (Mg blue, Al orange, H white, S yellow, O red, N blue, C gray and Hg purple).

attributed to Hg 4d3 (380.1 eV) compared with the original UTF (Fig. 6A-a), displaying that Hg^{2+} was bonded within the UTF *via* the complexation with Primuline. The removal of Hg^{2+} from the regenerated UTF by EDTA is confirmed by the absence of Hg signals (Fig. 6A-c). Compared with original (N=C: 399.8 eV; N—C: 402.1 eV) and regenerated one (N=C: 399.8 eV; N—C: 402.3 eV), the shift in the XPS peak for N 1s (N=C: 399.1 eV; N—C: 401.7 eV) of the Primuline/LDH UTF after measurement of Hg^{2+} indicates the formation of

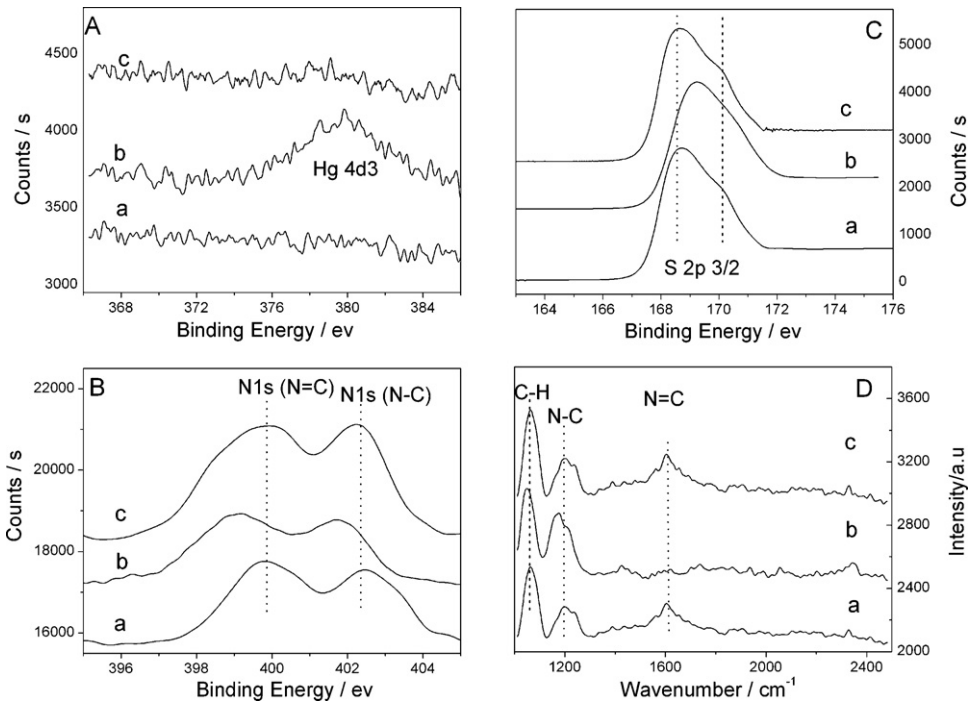

Fig. 6. (A–C) XPS spectra and (D) Raman spectra: (a) the original (Primuline/LDH)$_{25}$ UTF, (b) the treated UTF by Hg^{2+}, (c) the regenerated UTF by EDTA.

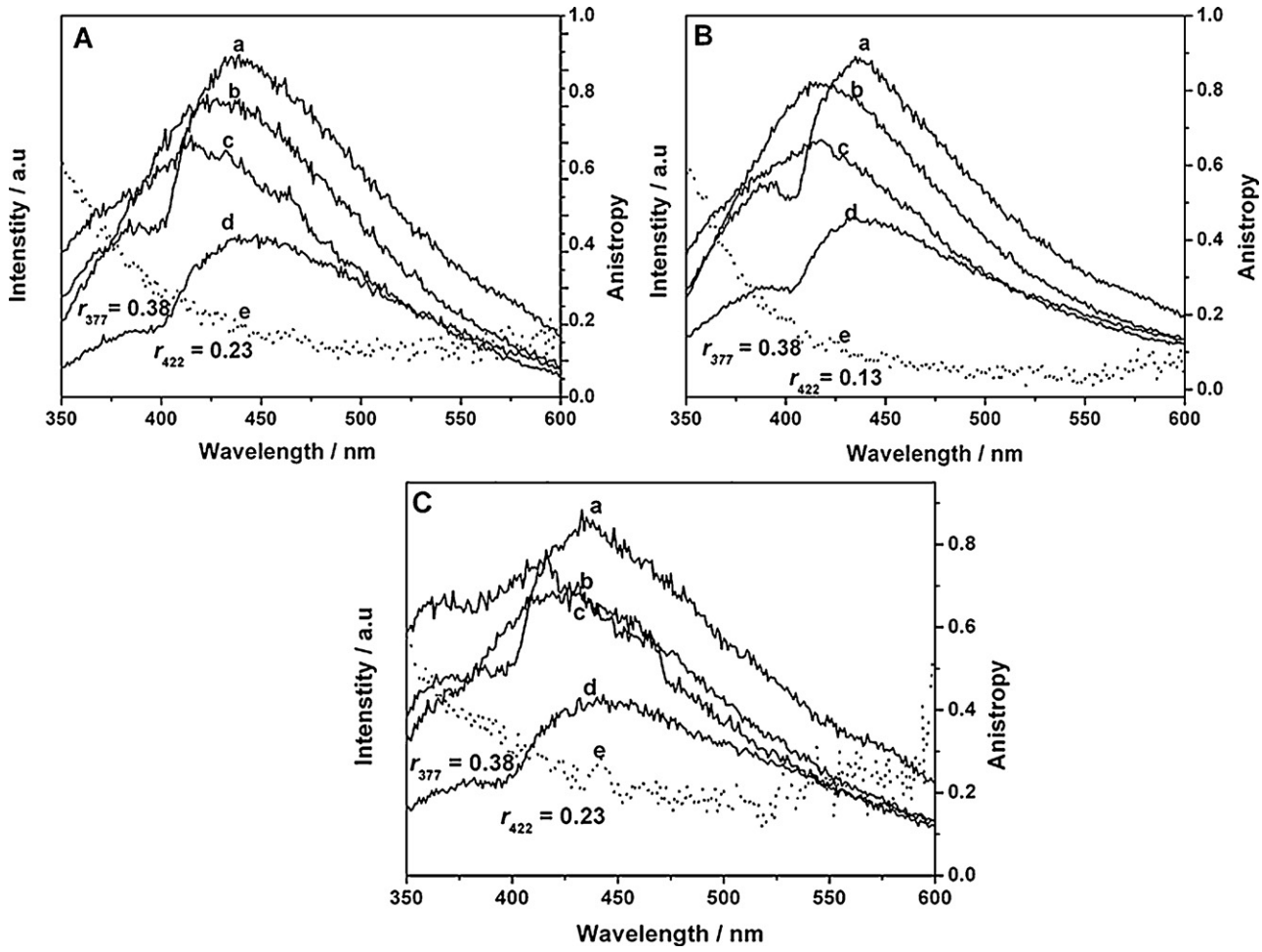

Fig. 7. Photoemission profiles in the (a) VV, (b) VH, (c) HV, (d) HH, (e) polarizations and anisotropy of the sample measured at room temperature (293 K): (a) the original $(Primuline/LDH)_{25}$ UTF, (b) the treated UTF by Hg^{2+} and (c) the regenerated UTF by EDTA.

coordination bond between Hg^{2+} and N atoms in Primuline (Fig. 6B). A similar shift in the banding energy of S 2p 3/2 was also observed (Fig. 6C), which can be attributed to the reduction of electron density [18]. In addition, Raman spectroscopy shows the absence of the C=N absorption and the band shift of C—H (from 1062 to 1045 cm^{-1}) and C—N (from 1200 to 1170 cm^{-1}) for the treated by Hg^{2+} compared with original and regenerated Primuline/LDH UTF, which further verified the results above (Fig. 6D).

The anisotropy of the $(Primuline/LDH)_{25}$ UTF is an another important information for illustration the mechanism of measurement–regeneration cycle. Fig. 7 shows the polarized photoemission spectra of the original, the treated and recovered $(Primuline/LDH)_{25}$ UTF samples. The well-defined fluorescence anisotropy of original $(Primuline/LDH)_{25}$ UTF with the anisotropy value (r) of 0.38 (377 nm) and 0.23 (422 nm) is observed in Fig. 7A, which caused by well-oriented and ordered arrangement of Primuline; while the r value decreased to 0.13 (422 nm) after measurement of Hg^{2+} (Fig. 7B) due to the decrease in the conjugacy of Primuline. The r value again recover to 0.23 after regeneration by EDTA (Fig. 7C), indicating the removal of Hg^{2+} from the UTF. In addition, AFM has also been used to confirm the reversible measurement–regeneration cycle and shown in Fig. S12. A smooth surface of the original $(Primuline/LDH)_{25}$ UTF with a root-mean square roughness of 3.46 nm is observed (Fig. S12A). However, after measurement of Hg^{2+}, the RMS roughness increases to 7.39 nm accompanied with sharp peaks (Fig. S12B). After regeneration by EDTA, the RMS roughness decreases to 3.58 nm (Fig. S12C). In conclusion, the embedment/removal of Hg^{2+} leads to reversible changes in both anisotropy and morphology owing to regular variations in orientation and/or stacking of Primuline.

4. Conclusions

In summary, the present work demonstrates a method for the fabrication of the ordered $(Primuline/LDH)_n$ UTFs by the LBL deposition technique, and their application as a ratiometric fluorescence chemosensor for Hg^{2+} was demonstrated. The structural and surface morphology studies show that the UTF is continuous and uniform with stacking order in the normal direction of the substrate. The rigid LDH nanosheets isolate Primuline molecules from each other and thus suppress the interlayer π–π stacking interaction. Furthermore, the $(Primuline/LDH)_{25}$ UTF is successfully used as ratiometric fluorescence chemosensor for Hg^{2+} with a low detection limit, good regeneration and reversibility, high stability (light, storage and mechanics) as well as selectivity. The reversible changes in chemical composition, surface morphology and fluorescence anisotropy of the UTF due to the embedment/removal of Hg^{2+} explain the mechanism of the measurement–regeneration cycle. Therefore, the novel strategy in this work provides a facile method for the fabrication of ratiometric fluorescence chemosensors *via* assembly of an organic fluorophore indicator within an inorganic matrix, which can be potentially used for the detection and measurement of toxic metal pollutants in biological and environmental detection.

Acknowledgments

This work was supported by the National Natural Science Foundation of China, the 863 Program (Grant No. 2009AA064201), the Fundamental Research Funds for the Central Universities.

Appendix A. Supplementary data

Supplementary data associated with this article can be found, in the online version, at http://dx.doi.org/10.1016/j.snb.2012.12.075.

References

[1] (a) Y.M. Sabri, R. Kojima, S.J. Ippolito, W. Wlodarski, K. Kalantar-zadeh, R.B. Kaner, S.K. Bhargava, QCM based mercury vapor sensor modified with polypyrrole supported palladium, Sensors and Actuators B: Chemical 160 (2011) 616–622;
(b) M. Kumar, N. Kumar, V. Bhalla, Rhodamine appended thiacalix[4]arene of 1,3-alternate conformation for nanomolar detection of Hg^{2+} ions, Sensors and Actuators B: Chemical 161 (2012) 311–316.

[2] (a) U.S. EPA, Regulatory Impact Analysis of the clean air mercury rule: EPA-452/R-05-003, 2005;
(b) H.H. Harris, I.J. Pickering, G.N. George, The chemical form of mercury in fish, Science 301 (2003) 1203.

[3] (a) M.A. Molina, J.R. Jiménez, M.D. Luque de Castro, Automated determination of mercury and arsenic in extracts from ancient papers by integration of solid-phase extraction and energy dispersive X-ray fluorescence detection using a lab-on-valve system, Analytica Chimica Acta 652 (2009) 148–153;
(b) Method 1631 Revision B: Mercury in water by oxidation, purge and trap, and cold vapor atomic fluorescence spectrometry, EPA-821-R-99-005, EPA, Office of Water, Washington, DC, May 1999;
(c) Y. Yang, Q. Zhao, W. Feng, F. Li, Luminescent chemodosimeters for bioimaging, Chemical Reviews (2012), http://dx.doi.org/10.1021/cr2004103;
(d) Q. Liu, J. Peng, C. Li, L. Sun, F. Li, High-efficiency upconversion luminescent sensing and bioimaging of Hg(II) by chromophoric ruthenium complex-assembled nanophosphors, ACS Nano 10 (2011) 8040–8048.

[4] (a) A. Le Bihan, J.Y. Cabon, L. Deschamps, P. Giamarchi, Imaging time-resolved electrothermal atomization laser-excited atomic fluorescence spectrometry for determination of mercury in seawater, Analytical Chemistry 83 (2011) 4881–4886;
(b) T. Frentiu, A.I. Mihaltan, M. Ponta, E. Darvasi, M. Frentiu, E. Cordos, Mercury determination in non-biodegradable materials by cold vapor capacitively coupled plasma microtorch atomic emission spectrometry, Journal of Hazardous Materials 193 (2011) 65–69;
(c) V.L. Dressler, F.G. Antes, C.M. Moreira, D. Pozebon, F.A. Duarte, As, Hg, I, Sb, Se and Sn speciation in body fluids and biological tissues using hyphenated-ICP-MS techniques, International Journal of Mass Spectrometry 307 (2011) 149–162.

[5] (a) K. Komatsu, Y. Urano, H. Kojima, T. Nagano, Development of an iminocoumarin-based zinc sensor suitable for ratiometric fluorescence imaging of neuronal zinc, Journal of the American Chemical Society 129 (2007) 13447–13454;
(b) H.H. Wang, L. Xue, C.L. Yu, Y.Y. Qian, H. Jiang, Rhodamine-based fluorescent sensor for mercury in buffer solution and living cells, Dyes Pigments 91 (2011) 350–355;
(c) F.J. Huo, J.J. Zhang, Y.T. Yang, A fluorescein-based highly specific colorimetric and fluorescent probe for hypochlorites in aqueous solution and its application in tap water, Sensors and Actuators B: Chemical 166 (2012) 44–49;
(d) N. Aksuner, E. Henden, I. Yilmaz, A novel optical chemical sensor for the determination of nickel (II) based on fluorescence quenching of newly synthesized thiazolo-triazol derivative and application to real samples, Sensors and Actuators B: Chemical 166 (2012) 269–274.

[6] (a) S. Sumalekshmy, M.M. Henary, N. Siegel, P.V. Lawson, Y. Wu, K. Schmidt, J.L. Bredas, J.W. Perry, C.J. Fahrni, Design of emission ratiometric metal-ion sensors with enhanced two-photon cross section and brightness, Journal of the American Chemical Society 129 (2007) 11888–11889;
(b) L. Xue, C. Liu, H. Jiang, A ratiometric fluorescent sensor with a large Stokes shift for imaging zinc ions in living cells, Chemical Communications 45 (2009) 1061–1063.

[7] (a) L. Xue, Z.J. Fang, G.P. Li, Ratiometric fluorescent sensors for detecting zinc ions in aqueous solution and living cells with two-photon microscopy, Sensors and Actuators B: Chemical 156 (2011) 410–415;
(b) M. Taki, J.L. Wolford, T.V. O'Halloran, Emission ratiometric imaging of intracellular zinc: design of a benzoxazole fluorescent sensor and its application in two-photon microscopy, Journal of the American Chemical Society 126 (2004) 712–713;
(c) M. Kumar, J.N. Babu, V. Bhalla, Ratiometric/'On-Off' sensing of Pb^{2+} ion using pyrene-appended calix[4]arenas, Sensors and Actuators B: Chemical 144 (2010) 183–191.

[8] V. Misra, H. Mishra, H.C. Joshi, An optical pH sensor based on excitation energy transfer in Nafion (R) film, Sensors and Actuators B: Chemical 82 (2002) 133–141.

[9] (a) Q. Wang, D. O'Hare, Recent advances in the synthesis and application of layered double hydroxide (LDH) nanosheets, Chemical Reviews 112 (2012) 4124–4155;
(b) G.R. Williams, D. O'Hare, Towards understanding, control and application of layered double hydroxide chemistry, Journal of Materials Chemistry 16 (2006) 3065–3074.

[10] (a) A.I. Khan, L.X. Lei, A.J. Norquist, D. O'Hare, Intercalation and controlled release of pharmaceutically active compounds from a layered double hydroxide, Chemical Communications 38 (2001) 2342–2343;
(b) A.M. Fogg, A.J. Freij, G.M. Parkinson, Synthesis and anion exchange chemistry of rhombohedral Li/Al layered double hydroxides, Chemistry of Materials 14 (2002) 232–234.

[11] (a) J.H. Choy, S.Y. Kwak, J.S. Park, Y.J. Jeong, J. Portier, Intercalative nanohybrids of nucleoside monophosphates and DNA in layered metal hydroxide, Journal of the American Chemical Society 121 (1999) 1399–1400;
(b) D.P. Yan, J. Lu, J. Ma, M. Wei, S. Qin, L. Chen, D.G. Evans, X. Duan, Thin film of coumarin-3-carboxylate and surfactant co-intercalated layered double hydroxide with polarized photoluminescence: a joint experimental and molecular dynamics study, Journal of Materials Chemistry 20 (2010) 5016–5024.

[12] (a) L. Enerbäck, K. Kristensson, T. Olsson, Cytophotometric quantification of retrograde axonal transport of a fluorescent tracer (Primuline) in mouse facial neurons, Brain Research 186 (1980) 21–32;
(b) Y. Oka, The origin of the centrifugal fibers to the olfactory bulb in the goldfish, *Carassius auratus*: an experimental study using the fluorescent dye Primuline as a retrograde tracer, Brain Research 185 (1980) 215–225.

[13] R.P. Bontchev, S. Liu, J.L. Krumhansl, J. Voigt, T.M. Nenoff, Synthesis, characterization, and ion exchange properties of hydrotalcite $Mg_6Al_2(OH)_{16}(A)_x(A')_{2-x}{\cdot}4H_2O$ (A,A′ = Cl^-, Br^-, I^- and NO_3^-, $2 \geq x \geq 0$) derivatives, Chemistry of Materials 15 (2003) 3669–3675.

[14] V.M. Martínez, F.L. Arbeloa, J.B. Prieto, T.A. López, I.L. Arbeloa, Characterization of supported solid thin films of laponite clay. Intercalation of rhodamine 6G laser dye, Langmuir 20 (2004) 5709–5717.

[15] World Health Organization. Guidelines for drinking-water quality: incorporating 1st and 2nd addenda, vol. 1, Recommendations, 3rd ed.; World Health Organization: Geneva, 2008. http://www.who.int/water_sanitation_health/dwq/fulltext.pdf (accessed 10.11.2010).

[16] J.D. Malhotra, L.H. Chen, Enhanced conjugated polymer fluorescence quenching by dipyridinium-based quenchers in the presence of surfactant, Journal of Physical Chemistry B 109 (2005) 3873–3878.

[17] S.I. Amer, Simplified removal of chelated metals, Metal Finishing 102 (2004) 36–40.

[18] G.X. Zhang, S.H. Sun, D.Q. Yang, J.P. Dodelet, E. Sacher, The surface analytical characterization of carbon fibers functionalized by H_2SO_4/HNO_3 treatment, Carbon 46 (2008) 196–205.

Biographies

Hao Chen is a master student in the College of Science, Beijing University of Chemical Technology. His research interest is fabricating inorganic–organic composite film for various sensing applications.

Xiaolan Ji is a master student in the College of Science, Beijing University of Chemical Technology. Her research interest is fabricating inorganic–organic composite film for various sensing applications.

Shitong Zhang is a PhD student in the College of Science, Beijing University of Chemical Technology. His research interest is theory study on inorganic–organic composite materials.

Wenying Shi received her PhD from Beijing University of Chemical Technology in 2010. She is a teacher in the State Key Laboratory of Chemical Resource Engineering and the College of Science in Beijing University of Chemical Technology. Her main research interests are in the fabrication and application of the organic–inorganic photoluminescence film materials.

Min Wei received her PhD from Peking University in 2001. She is a full professor in the State Key Laboratory of Chemical Resource Engineering and the College of Science in Beijing University of Chemical Technology. Her main research interests are in supramolecular assembly chemistry, functional intercalated materials, and the development of organic–inorganic photoluminescence film materials.

David G. Evans is a British chemist. He is a special engaged professor in the State Key Laboratory of Chemical Resource Engineering and the College of Science in Beijing University of Chemical Technology. Her main research interests are in basic or applied research of the layered materials.

Xue Duan is an academician of the Chinese Academy of Sciences. He is a full professor in the State Key Laboratory of Chemical Resource Engineering and the College of Science in Beijing University of Chemical Technology. Her main research interests are in intercalation assembly and product engineering.